Cell, Vol. 123, 37–48, October 7, 2005, Copyright ©2005 by Elsevier Inc. DOI 10.1016/j.cell.2005.08.002

The Polyadenylation Factor CPSF-73 Is Involved in Histone-Pre-mRNA Processing

Zbigniew Dominski,* Xiao-cui Yang, and William F. Marzluff

Department of Biochemistry and Biophysics and Program in Molecular Biology and Biotechnology
University of North Carolina at Chapel Hill
Chapel Hill, North Carolina 27599

Summary

During 3′ end processing, histone pre-mRNAs are cleaved 5 nucleotides after a conserved stem loop by an endonuclease dependent on the U7 small nuclear ribonucleoprotein (snRNP). The upstream cleavage product corresponds to the mature histone mRNA, while the downstream product is degraded by a 5′-3′ exonuclease, also dependent on the U7 snRNP. To identify the two nuclease activities, we carried out UV-crosslinking studies using both the complete RNA substrate and the downstream cleavage product, each containing a single radioactive phosphate and a phosphorothioate modification at the cleavage site. We detected a protein migrating at 85 kDa that crosslinked to each substrate in a U7-dependent manner. Immunoprecipitation experiments identified this protein as CPSF-73, a known component of the cleavage/polyadenylation machinery. These studies suggest that CPSF-73 is both the endonuclease and 5′-3′ exonuclease in histone-pre-mRNA processing and reveal an evolutionary link between 3′ end formation of histone mRNAs and polyadenylated mRNAs.

Introduction

3′ end processing of nuclear pre-mRNAs is an essential step in formation of mature mRNAs. The vast majority of pre-mRNAs undergo cleavage coupled to poly(A) addition (Zhao et al., 1999). In contrast, cleavage of metazoan replication-dependent histone pre-mRNAs occurs by a different mechanism and is not followed by polyadenylation (Dominski and Marzluff, 1999). Each type of pre-mRNA contains specific sequence elements that are recognized by a unique set of processing factors. Histone pre-mRNAs contain two sequence elements required for processing: (1) the stem loop consisting of a 6 base pair stem and a 4 nucleotide loop and (2) a histone downstream element (HDE). Cleavage occurs between the two elements, 5 nucleotides downstream of the stem loop. The HDE is the binding site for the U7 snRNP, which consists of an ~60 nucleotide snRNA and a number of proteins, including the U7 snRNP-specific proteins Lsm10 and Lsm11 (Schumperli and Pillai, 2004). Binding of U7 snRNP to the pre-mRNA is mediated by formation of a duplex between the HDE and the 5′ end of the U7 snRNA (Birnstiel and Schaufele, 1988; Bond et al., 1991). The stem-loop binding protein (SLBP) binds the stem loop and stabilizes the U7 snRNP on the pre-mRNA by interacting with a component of the U7 snRNP, ZFP100 (Dominski et al., 2002). In processing of mammalian histone pre-mRNAs, the cleavage site is located at a fixed distance from the HDE, suggesting that the U7 snRNP plays a key role in recruiting the endonuclease to the pre-mRNA (Scharl and Steitz, 1994). A main focus of current studies is to identify this elusive factor directly responsible for cleaving histone pre-mRNAs.

Cleavage coupled to polyadenylation is carried out by a large complex consisting exclusively of protein factors that include the multisubunit cleavage/polyadenylation specificity factor (CPSF) and cleavage stimulation factor (CstF) (Colgan and Manley, 1997). It is now believed that cleavage coupled to polyadenylation is catalyzed by CPSF-73, a subunit of CPSF (Ryan et al., 2004). Here we report the results of UV-crosslinking studies designed to identify proteins that contact histone pre-mRNA in the vicinity of the cleavage site. We detected an 85 kDa protein, which is crosslinked to the histone pre-mRNA in a processing-dependent manner. Immunoprecipitation experiments identified this protein as CPSF-73, strongly suggesting that histone pre-mRNAs as well as the other pre-mRNAs that undergo cleavage/polyadenylation utilize the same endonuclease during 3′ end processing.

Results

In Vitro 3′ End Processing of Histone pre-mRNAs

In vitro 3′ end processing of histone pre-mRNAs in mammalian nuclear extracts occurs readily in the presence of 20 mM EDTA at 32°C (Gick et al., 1986). We routinely use the mouse histone H2A-614 pre-mRNA as the processing substrate (Figure 1A) and nuclear extracts from mouse myeloma cells (Dominski et al., 1999). The HDE in the H2A-614 pre-mRNA forms a stable duplex with the 5′ end of the U7 snRNA consisting of 14 base pairs interrupted by only one mismatch. As a result of strong binding with the U7 snRNP, the H2A-614 pre-mRNA is cleaved in vitro even in the presence of the stem-loop RNA sequestering all SLBP (Figure 1C, lanes 2 and 3). Processing of histone pre-mRNAs is specifically abolished by a 2′-O-methyl oligonucleotide, αMa, complementary to the first 17 nucleotides of the mouse U7 snRNA (Figures 1B and 1C, lane 4). The U7 snRNP is present at low concentrations in the nucleus, and an excess of pre-mRNA saturates the in vitro reaction, resulting in poor processing efficiency. Addition of 10-fold excess of unlabeled pre-mRNA substrate reduces processing of the labeled pre-mRNA to 10% of its initial level (Figure 1C, lane 6). Cleavage of the H2A-614 pre-mRNA occurs after the ACCCA (Scharl and Steitz, 1994), leaving a 3′ hydroxyl group on the upstream fragment containing the stem loop (SL) and 5′ phosphate on the downstream cleavage product (DCP) starting with CU (Figure 1A). The DCP, visible only when the substrate is internally labeled, is degraded by an EDTA-resistant 5′-3′ exonuclease that is also de-

*Correspondence: dominski@med.unc.edu

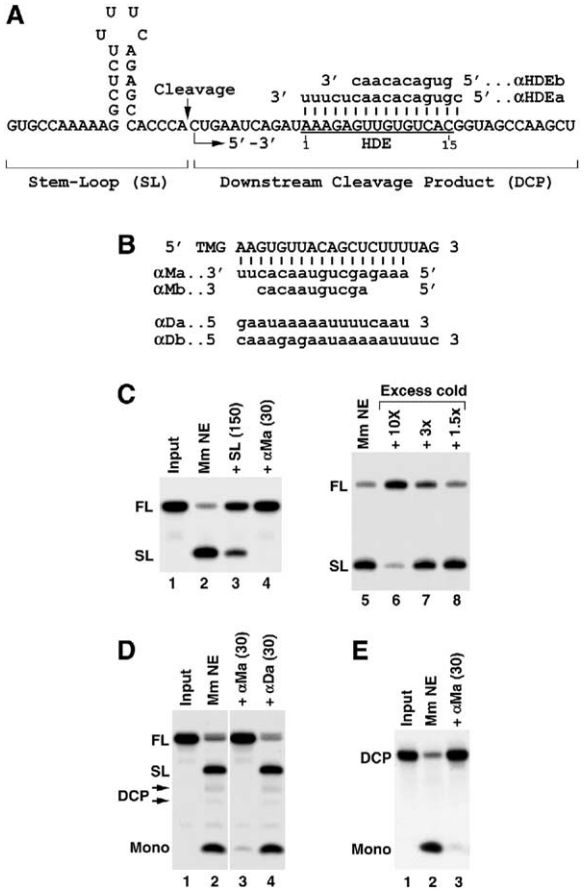

Figure 1. In Vitro 3′ End Processing of Histone pre-mRNAs

(A) The sequence of the mouse H2A-614 pre-mRNA encompassing the stem loop (SL) and the downstream cleavage product (DCP) containing the histone downstream element (HDE) (underlined and numbered) that base pairs with the U7 snRNA. The site of endonucleolytic cleavage and the direction of exonucleolytic degradation of the DCP are indicated with arrows. The sequences of two 2′-O-methyl oligonucleotides complementary to the HDE are shown above.

(B) The sequence of the 5′ end of the mouse/human U7 snRNA starting with the trimethyl guanosine cap (TMG) and the sequences (written in the 3′-5′ orientation) of two anti-U7 oligonucleotides (αMa and αMb) complementary to this region. Vertical lines indicate base pairs. The sequences of two control 2′-O-methyl oligonucleotides, αDa and αDb (written in the 5′-3′ orientation), complementary to the *Drosophila* U7 snRNA are shown below.

(C) In vitro processing of 0.1 pmol of a 5′-labeled mouse H2A-614 pre-mRNA in a nuclear extract from mouse myeloma cells (Mm NE). The competitors used to affect processing are indicated at the top of each lane. The numbers in parentheses indicate the amount of the RNA competitors in pmol. FL and SL indicate the input H2A-614 pre-mRNA and the upstream cleavage product, respectively.

(D) In vitro processing of a uniformly labeled H2A-614 pre-mRNA in Mm NE. Arrows indicate partial degradation products of the downstream cleavage product (DCP) ultimately converted to mononucleotides.

(E) Release of the 5′ label from the DCP in Mm NE by a U7 snRNP-dependent mechanism.

pendent on the U7 snRNP (Walther et al., 1998). The degradation of the DCP is often incomplete, resulting in accumulation of a number of intermediates partially truncated at the 5′ end in addition to mononucleotides (Figure 1D, lanes 2–4, arrows). A synthetic RNA encompassing the DCP not protected at the 5′ end by the cap structure is degraded in nuclear extracts by the same activity, demonstrating that the endonucleolytic cleavage and the 5′-3- degradation can be uncoupled (Figure 1E) (Walther et al., 1998).

Processing and UV Crosslinking Using the Full-Length Substrate

To identify the endonuclease that cleaves histone pre-mRNAs, we carried out UV-crosslinking experiments using site-specifically labeled RNA substrates. We assumed that formation of a crosslink between the nuclease and the RNA substrate should correlate with processing efficiency. To selectively abolish processing, we used two 2′-O-methyl oligonucleotides, αMa and αMb, complementary to either 17 or 11 nucleotides of the 5′ end of the mouse U7 snRNA (Figure 1B). In addition to the oligonucleotides blocking the U7 snRNA, we also used two 2′-O-methyl oligonucleotides complementary to 16 (αHDEa) or 10 nucleotides (αHDEb) of the HDE (Figure 1A). These oligonucleotides act in *cis* by blocking the site of binding for U7 snRNA on the pre-mRNA and also efficiently inhibit processing. We consider this control as less informative than the anti-mouse U7 snRNA oligonucleotides since formation of a duplex spanning a significant portion of the RNA substrate might also affect nonspecific binding of proteins to the substrate.

To generate a site-specifically labeled full-length pre-mRNA, a 31 nucleotide upstream fragment containing the stem loop and followed by the ACCCA (SL) was ligated to a 5′-labeled 38 nucleotide downstream cleavage product (DCP) that contained the U7 binding site from the H2A-614 pre-mRNA (Figure 1A). The full-length RNA (FL) containing a single ^{32}P at the cleavage site (Figure 2A) was gel purified, and approximately 0.1 pmol (10,000 counts per minute) used for processing in a mouse nuclear extract (Mm NE). Each processing sample was preincubated at 32°C for 10 min, and then the majority of the sample was UV irradiated at room temperature, treated with RNase A, and analyzed by SDS gel electrophoresis for the formation of crosslinks. A small aliquot was incubated at 32°C for an additional 80 min, and the RNA was isolated to measure the processing efficiency in 7 M urea gels. Following processing, the upstream product containing the stem loop is not detected by autoradiography since the radioactive phosphate remains at the 5′ end of the DCP, which is degraded in a 5′-3′ orientation, resulting in a labeled mononucleotide. Thus, processing efficiency for this substrate is measured by gradual disappearance of the substrate and accumulation of mononucleotides (Figure 2A, lane 2). Processing was abolished by the αMa and was unaffected by a control oligonucleotide (αD) complementary to the first 17 nucleotides of the *Drosophila* U7 snRNA (lanes 3 and 4). In spite of processing of 85% of the input pre-mRNA, UV irradiation did not generate any RNA-protein crosslink that was dependent on U7 snRNP (data not shown).

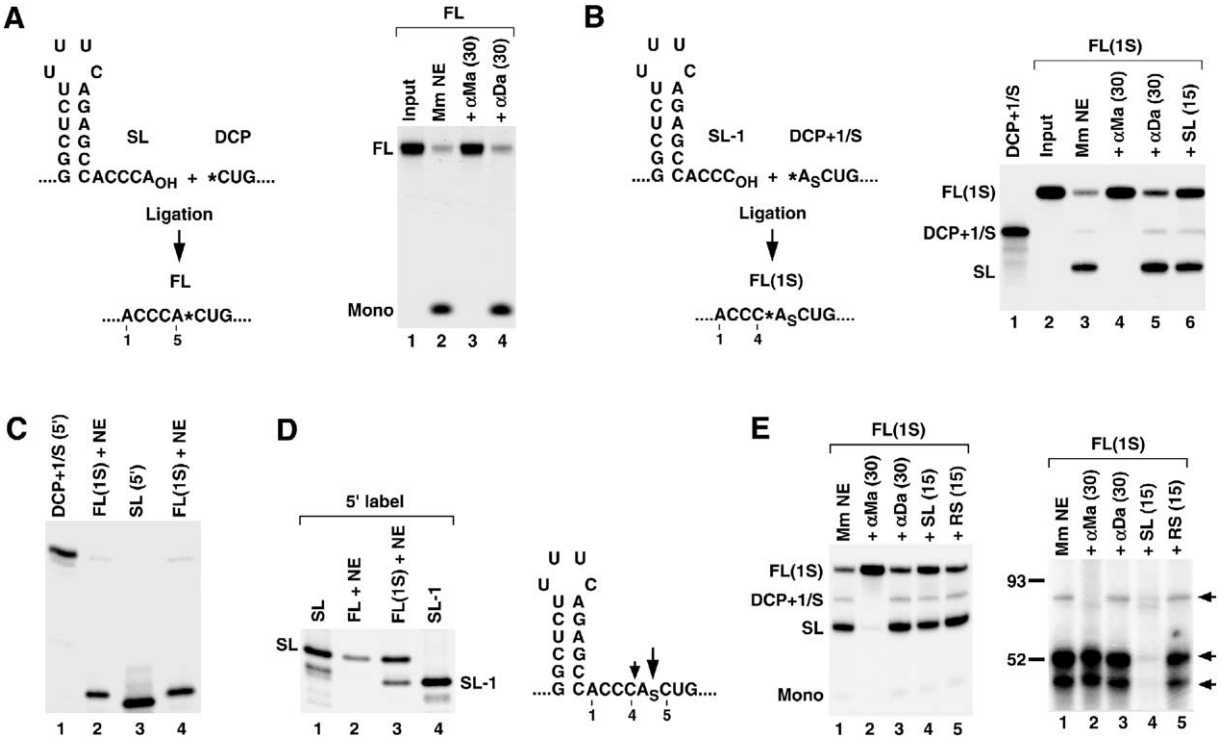

Figure 2. 3′ End Processing and UV Crosslinking Using the Full-Length RNA Substrates

(A) Left panel: diagram of construction of the full-length (FL) substrate with a radiolabeled phosphate (asterisk) at the cleavage site. Only partial sequences of the SL and DCP RNAs are shown. The first and the fifth nucleotides after the stem are indicated with numbers. Right panel: in vitro processing of the gel-purified FL pre-mRNA in Mm NE (lanes 2–4) in the presence of the indicated amounts (pmol) of competitors.

(B) Left panel: diagram of construction of the FL(1S) RNA containing the phosphorothioate modification (S) at the cleavage site and a radiolabeled phosphate (asterisk) 1 nucleotide upstream. Right panel: in vitro processing of the FL(1S) RNA in Mm NE (lanes 3–6) in the presence of the indicated amounts (pmol) of competitors. The 5′-labeled DCP+1/S used in RNA ligation is shown in lane 1 and the FL(1S) substrate in lane 2.

(C) High-resolution gel electrophoresis of processing products of the site-specifically labeled FL(1S) RNA generated in a mouse NE (lanes 2 and 4). The 5′-labeled DCP+1/S (lane 1) and SL RNAs (lane 3) are used as size standards.

(D) Left panel: high-resolution gel electrophoresis of processing products of the 5′-labeled FL (lane 2) and FL(1S) RNAs (lane 3) generated in a mouse NE. The 5′-labeled SL and SL–1 (lanes 1 and 4) were used as size standards. Right panel: the position of the cleavage sites in the FL(1S) RNA.

(E) Processing (left panel) and UV crosslinking (right panel) using the FL(1S) RNA. The numbers in parentheses above each lane indicate the amounts of each competitor in pmol (lanes 2–5). The RS RNA is the reverse stem mutant of the SL RNA unable to bind SLBP. The specific crosslinks, which correlate with processing, are indicated with arrows (right panel).

Processing and UV Crosslinking Using the Full-Length Substrate Containing a Phosphorothioate

One possible explanation for the failure to detect any U7-dependent crosslinks on the FL RNA could have been the rapid rate of the catalysis. To overcome this potential limitation, the scissile bond was changed by introduction of a phosphorothioate, a modification that increases resistance of nucleic acids to nucleases (Koziolkiewicz et al., 1997). We reasoned that this modification might slow down the kinetics of the cleavage reaction, thus providing a sufficient time window to crosslink the endonuclease while it was in contact with the RNA. To place the phosphorothioate at the scissile bond, the DCP was extended at the 5′ end by an adenosine, and the modification (S) was introduced within the first phosphodiester bond (Figure 2B). To emphasize extension of the typical downstream cleavage product by 1 nucleotide and the presence of 1 phosphorothioate, we refer to this RNA as DCP+1/S. The 5′-labeled DCP+1/S RNA was ligated to the stem-loop fragment lacking the last nucleotide (SL–1). In the ligated FL(1S) RNA, the phosphorothioate modification was at the cleavage site, and the radioactive phosphate was 1 nucleotide upstream, between a cytosine and an adenosine. Processing of the gel-purified FL(1S) generated a major product that contained the radioactive phosphate and had the mobility of the SL RNA (Figure 2B, lane 3), thus suggesting that cleavage predominantly occurred either at the regular cleavage site or slightly further downstream. There was also a small amount of a product comigrating with the DCP+1/S, indicating that the presence of the phosphorothioate resulted in generation of a minor cleavage site upstream of the normal cleavage site, leaving the label on the DCP. Generation of both products was nearly completely inhibited in the presence of 30 pmol of the αMa

oligonucleotide, whereas the αDa had no effect (Figure 2B, lanes 4 and 5). The SL competitor reduced processing at the major cleavage site from 75% to about 40% and had no detectable effect on processing at the minor site (lane 6).

To precisely map the sites of cleavage in the FL(1S) RNA, the processing products were separated on a high-resolution polyacrylamide gel next to the SL, SL–1, and DCP+1/S labeled at the 5′ end. The less abundant processing product comigrated with the DCP+1/S (note that both RNAs contain a labeled phosphate at the 5′ end), demonstrating that the minor cleavage site is located 1 nucleotide upstream of the regular cleavage site, between the cytidine and adenosine (Figure 2C, lanes 1 and 2). The major cleavage product (containing the internal radioactive phosphate and no phosphate at the 5′ end) migrated slightly more slowly than the SL (lanes 2–4), and this difference is either due to the lack of the 5′ phosphate (Sollner-Webb et al., 2001) or to cleavage occurring 1 nucleotide downstream of the regular cleavage site. Importantly, the latter possibility would indicate that the presence of phosphorothioate at the normal cleavage site resulted in the shifting of the cleavage 1 nucleotide in either direction. To discriminate between these two possibilities, we generated an unlabeled FL(1S) RNA by ligating the SL–1 and the 5′-phosphorylated DCP+1/S. As a control, we also generated an unlabeled FL RNA lacking the phosphorothioate by ligating the SL and the 5′-phosphorylated DCP. Both RNAs were labeled at the 5′ end, and their processing products were separated on a high-resolution gel. Consistent with previous results, the control FL RNA was cleaved only at the normal site generating the upstream product comigrating with the 5′-labeled SL (Figure 2D, lanes 1 and 2). As expected from the previous analysis, the FL(1S) RNA containing the modification was cleaved at two sites. The major product had the same mobility as the SL, and the minor product was 1 nucleotide shorter, comigrating with the 5′-labeled SL–1 (Figure 2D, lanes 3 and 4). We conclude from these experiments that the FL(1S) containing the phosphorothioate in the cleavage site is processed with about 70% efficiency at this site, although the presence of the modification results in cleavage of 30% of the substrate 1 nucleotide upstream (Figure 2D, right).

We next tested the ability of the FL(1S) RNA to form processing-dependent RNA-protein crosslinks. To avoid removal of the radioactive phosphate from proteins crosslinked to the RNA, prior to separating on an SDS gel, the UV-irradiated processing reactions were treated with RNase T1, cleaving after guanosines, instead of RNase A, which cleaves after pyrimidines and might remove the label from the adenosine crosslinked to the protein. Three RNA-protein crosslinks migrating at 45, 52, and 85 kDa (Figure 2E, right, arrows) were generated in a control processing reaction, and none of the crosslinks were affected by control oligonucleotides unable to bind the mouse U7 snRNA (αD, lane 3) or SLBP (RS, lane 5). Excess SL eliminated formation of the two major bands migrating at 45 and 52 kDa, indicating that they likely represent crosslinked SLBP (Figure 2E, right-hand panel, lane 4). Importantly, there was a less intense crosslink migrating at 85 kDa, formation

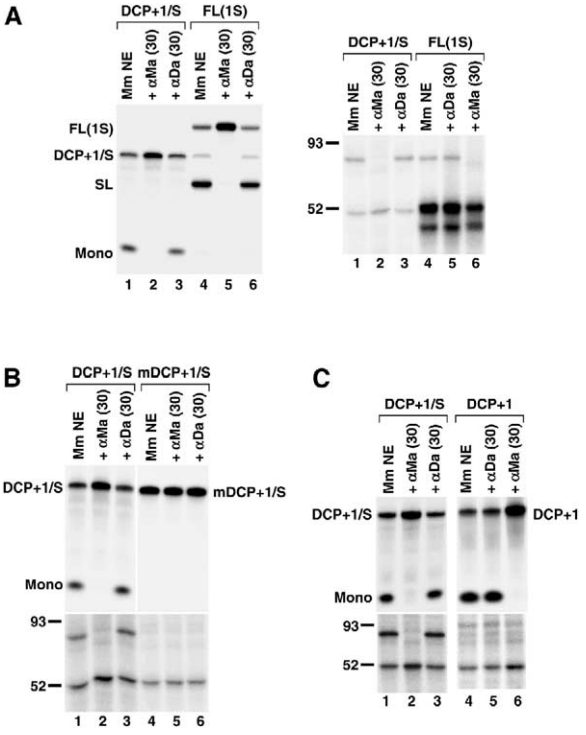

Figure 3. UV Crosslinking to the FL(1S) and DCP+1/S RNAs and Preliminary Characterization of the 85 kDa Crosslink

(A) Formation of processing products (left) and crosslinks (right) using DCP+1/S (lanes 1–3) or FL(1S) RNAs (lanes 4–6) as substrates in Mm NE. The numbers in parentheses indicate amounts of each competitor in pmol. Note that the order of samples in the right panel has been switched in lanes 5 and 6.

(B) U7-dependent release of the 5′-labeled mononucleotide (top) and crosslink formation (bottom) using DCP+1/S (lanes 1–3) or mutant mDCP+1/S (lanes 4–6) as substrates in Mm NE in the presence of the indicated competitors.

(C) U7-dependent release of the 5′-labeled mononucleotide (top) and crosslink formation (bottom) using DCP+1/S (lanes 1–3) or DCP+1 lacking the phosphorothioate (lanes 4–6) as substrate in Mm NE in the presence of the indicated competitors.

of which was abolished by the αMa and significantly reduced by the presence of the SL (Figure 2E, right, lanes 2 and 4), thus demonstrating the correlation between crosslinking and processing expected for the cleavage factor (Figure 2E, left).

UV Crosslinking to the FL(1S) and DCP+1/S RNAs and Preliminary Characterization of the 85 kDa Crosslink

The HDE from the H2A-614 pre-mRNA can efficiently bind the U7 snRNP in the absence the stem loop and SLBP (Dominski et al., 1999). Therefore, we compared the pattern of crosslinking with the DCP+1/S labeled at the 5′ end to that seen with the FL(1S) RNA. A labeled mononucleotide was rapidly released from the DCP+1/S RNA incubated in a mouse nuclear extract, and the reaction required U7 snRNP since it was completely inhibited by the αMa but unaffected by the αD (Figure 3A, left-hand panel, lanes 1–3). The FL(1S) RNA gave the same two cleavage products observed in Figure 2B

(Figure 3A, left-hand panel, lanes 4–6). After UV irradiation and RNase T1 treatment, the processing reactions were analyzed for generation of RNA-protein crosslinks. Two crosslinks were detected with the DCP+1/S substrate: a U7-dependent 85 kDa protein that comigrated with the 85 kDa crosslink formed on the FL(1S) RNA and a new crosslink that migrated at about 50 kDa, just below the major stem-loop-dependent crosslink formed on the FL(1S) RNA (Figure 3A, right-hand panel). The 50 kDa crosslink was not affected by the presence of either the αMa or αD oligonucleotides, whereas the 85 kDa crosslink was abolished by the αMa.

Since the 5′-labeled DCP+1/S was readily available in large quantities, we used this substrate to further characterize the UV-crosslinked proteins. In contrast to the FL(1S) RNA, in which the radioactive phosphate is preceded by a cytosine, the DCP+1/S contains the radioactive phosphate on the first nucleotide, an adenosine, and thus it can be digested with RNase A without risk of removing the label from the crosslinked proteins. Indeed, the same two protein crosslinks of 85 kDa and 50 kDa were detected with the DCP+1/S substrate when RNase A was used instead of RNase T1 (see Figure S1A in the Supplemental Data available with this article online). A nuclear extract from HeLa cells was also capable of forming the 85 kDa crosslink with the DCP+1/S, although its efficiency was much lower than for mouse nuclear extracts. This lower efficiency of crosslinking of the 85 kDa protein correlated with much lower activity of HeLa nuclear extracts in releasing the radioactive mononucleotide from the DCP+1/S (Figure S1B). Detection of the 85 kDa crosslink absolutely required a 5–10 min preincubation of samples at 32°C, whereas subsequent UV irradiation could be carried with the same result at either room temperature or on ice (Figure S1C).

To further demonstrate that crosslinking of the 85 kDa protein depends on binding of U7 snRNP, we used a mutant RNA substrate unable to form a strong duplex with U7 snRNA. We mutated the purine core AAGA in the DCP+1/S (Figure 1A, nucleotides 2–5 of the HDE) to UUCA, thus significantly limiting the base-pairing potential between the RNA substrate and the U7 snRNA. The mDCP+1/S mutant RNA labeled at the 5′ end was stable in a mouse nuclear extract (Figure 3B, top, lanes 4–6) and formed only the 50 kDa crosslink and not the 85 kDa crosslink, emphasizing the importance of the interaction between the RNA substrate and the U7 snRNP for recruitment of the 85 kDa protein and release of the labeled mononucleotide (Figure 3B, bottom, lanes 4–6). To prove that generation of the 85 kDa protein crosslink was due to introduction of the phosphorothioate, we used an RNA substrate of the same length and sequence as the DCP+1/S but lacking the phosphorothioate modification (DCP+1). The radioactive label was efficiently removed from the 5′ end of the DCP+1 RNA substrate during the 90 min incubation in a mouse nuclear extract, but only the 50 kDa protein crosslink was detected (Figure 3C, lanes 4–6). Based on this result, we conclude that the presence of the phosphorothioate modification is a prerequisite for efficient crosslinking of the 85 kDa protein.

Specificity of UV Crosslinking to the DCP+1/S

We used various RNA and 2′-O-methyl competitors to test the correlation between formation of the 85 kDa and 50 kDa crosslinks and release of the 5′-labeled adenosine from the DCP+1/S RNA. In addition to the αMa, we used αHDEa, a 2′-O-methyl oligonucleotide complementary to 16 nucleotides of the HDE (Figure 1A). Removal of the labeled mononucleotide from the DCP+1/S RNA as well as formation of both the 85 and 50 kDa crosslinks was abolished in the presence of 10 pmol of the HDEa, a 100-fold molar excess over the substrate (Figure 4A, lane 2). None of the nonspecific RNA competitors, used in amounts ranging from 15 to 300 pmol, including the SL RNA, the RS RNA, and a 20-mer 2′-O-methyl oligonucleotide complementary to the *Drosophila* U7 snRNA (αDb), had any effect on either the release of the labeled mononucleotide from the DCP+1/S or formation of the 85 and 50 kDa crosslinks (Figure 4A, lanes 3–8). Note that excess of the SL RNA had no effect on crosslinking of the 85 kDa protein to the DCP+1/S RNA, although it had a significant effect on formation of the same crosslink on the full-length RNA FL(1S) (Figure 2E, right-hand panel). This result is consistent with the lack of the stem loop in the DCP+1/S substrate and the release of the labeled mononucleotide occurring in an SLBP-independent manner.

We also tested the effect of two shorter 2′-O-methyl oligonucleotides: αMb, complementary to 11 nucleotides of the mouse U7 snRNA, and αHDEb, complementary to 10 nucleotides of the HDE (Figures 1A and 1B). The αMb at 40 and 4 pmol was a very potent inhibitor of the RNA processing and formation of the crosslink to the 85 kDa protein (Figure 4B, lanes 2 and 3; Figure 5C, lane 2) and at 0.4 pmol was partially effective (Figure 4B, lane 4; Figure 5C, lane 3). The αHDEb at 20 pmol almost entirely blocked release of the 5′-labeled adenosine and crosslinking of the 85 kDa and 50 kDa proteins, while 2 pmol had a moderate effect (Figure 4B, lanes 5 and 6). The release of the mononucleotide from the DCP+1/S RNA and crosslinking of the 85 kDa protein were abolished by the excess of the unlabeled substrate, confirming that the nuclease cleaving off the 5′ adenosine depends on a limiting factor, most likely the U7 snRNP (lanes 8–10). Consistent with this, 200 pmol of the mDCP+1/S RNA, more than a 1000-fold excess over the labeled RNA, did not reduce the amount of the mononucleotide and formation of the 85 kDa crosslink, although crosslinking of the 50 kDa protein was abolished (Figure 4C, lane 5). Clearly, the interaction of the 50 kDa protein with the substrate is not required for release of the mononucleotide from the DCP+1/S RNA. We also tested as competitors a number of previously characterized full-length pre-mRNAs consisting of the stem loop and different HDE sequences. Two of these substrates, *Drosophila*-specific H3 pre-mRNA and HDE^{-} mutant of the H2A pre-mRNA, are not processed in mammalian extracts since they do not interact stably with the U7 snRNP, and the third substrate, the mouse H1t pre-mRNA, is processed poorly due to weak binding of the U7 snRNP (Dominski et al., 1999). The wild-type H2A-614 pre-mRNA at a 25-fold molar excess over the labeled RNA substrate nearly completely abolished processing and generation of the 85 kDa crosslink (Figure 4C, lane 7). The three

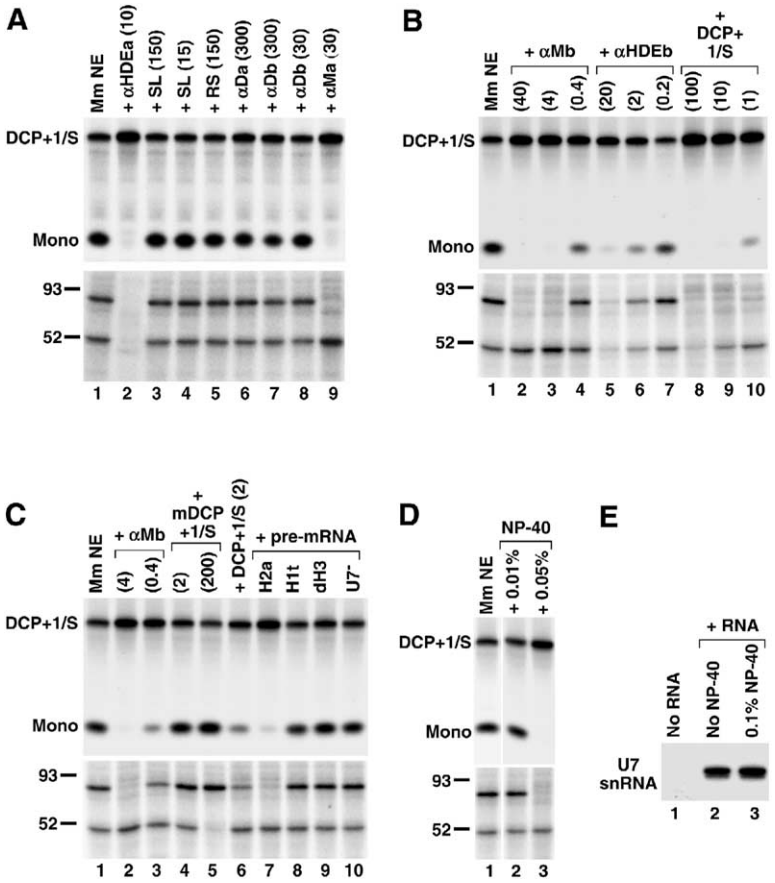

Figure 4. Specificity of UV Crosslinking to the DCP+1/S

(A–C) Effects of various competitors indicated at the top of each lane on release of the 5′-labeled mononucleotide (top) and crosslink formation (bottom) in Mm NE using the DCP+1/S RNA as a substrate. Numbers in parentheses indicate the amount of the RNA competitors in pmol.

(D) Effects of NP-40 on release of the 5′-labeled mononucleotide (top) and crosslink formation (bottom) in Mm NE using the DCP+1/S RNA as a substrate.

(E) Northern blot analysis of the mouse U7 snRNA in processing complexes formed in either the absence (lane 1) or presence of the H2A-614 pre-mRNA (lanes 2 and 3). Processing complexes were precipitated by anti-SLBP and collected on protein A agarose beads in either the absence (lane 2) or presence of 0.1% NP-40 (lane 3), and the amount of U7 snRNA was determined by Northern blotting.

remaining RNAs, the H1t, the *Drosophila* H3, and the HDE⁻ mutant, at the same molar concentration had no effect on processing and crosslinking (Figure 4C, lanes 8–10). Taken together, these results clearly demonstrate that formation of the 85 kDa crosslink is dependent on the ability of the substrate to efficiently bind the U7 snRNP.

We have observed that increasing the concentrations of NP-40 over 0.025% abolished processing of the H2A-614 pre-mRNA, although 0.01% NP-40 had no effect (data not shown). Interestingly, concentration as high as 0.1% does not affect the amount of the U7 snRNA detected in processing complexes assembled on the H2A-614 pre-mRNA (Figure 4E, lanes 2 and 3), suggesting that NP-40 interferes with a step other than the binding of the U7 snRNP. We tested effects of 0.01% and 0.05% NP-40 on degradation of the DCP+1/S RNA and crosslinking of the 85 kDa protein. While the release of the mononucleotide from the DCP+1/S and crosslinking of the 85 kDa protein were not affected in the presence of 0.01% NP-40, both events were fully inhibited by 0.05% NP-40 (Figure 4D, lanes 2 and 3). Therefore, it is likely that NP-40 may have a direct effect on recruiting the 85 kDa protein to the DCP+1/S by the U7 snRNP stably associated with the RNA. Alternatively, NP-40 causes dissociation of a loosely associated component from the U7 snRNP that is required for recruitment of the 85 kDa protein.

Distinguishing between the Endonucleolytic and the 5′-3′ Exonucleolytic Activities

Two different mechanisms, leading to the same product, could be responsible for the release of the radioactive 5′ nucleotide from the DCP+1/S RNA: a 5′-3′ exonucleolytic degradation or an endonucleolytic cleavage followed by the 5′ exonucleolytic degradation of the DCP, as in the case of natural histone pre-mRNAs. Since it is not possible to discriminate between these two mechanisms using the DCP+1/S RNA, we used two other RNA substrates in which the DCP sequence was extended at the 5′ end by either 5 (DCP+5/S) or 6 nucleotides (DCP+6/5S) preceding the normal cleavage site (Figure 5A). The DCP+5/S RNA contained the phosphorothioate modification at the normal cleavage site between an adenosine and cytidine, while DCP+6/5S had four additional phosphorothioates, two on each side of the cleavage site. When these RNA substrates labeled at the 5′ end were incubated in a mouse nuclear extract, the same U7-dependent release of the radioactive mononucleotide was observed as in the case of the DCP+1/S (Figure 5B). The reaction occurs in the presence of EDTA, which stabilizes the upstream cleavage product, thus making it unlikely that the HDC+5/S and DCP+6/5S are endonucleolytically cleaved further away from the 5′ end followed by degrading the resultant upstream product to mononucleotides by a 3′-5′ exonuclease. This result demonstrates that mov-

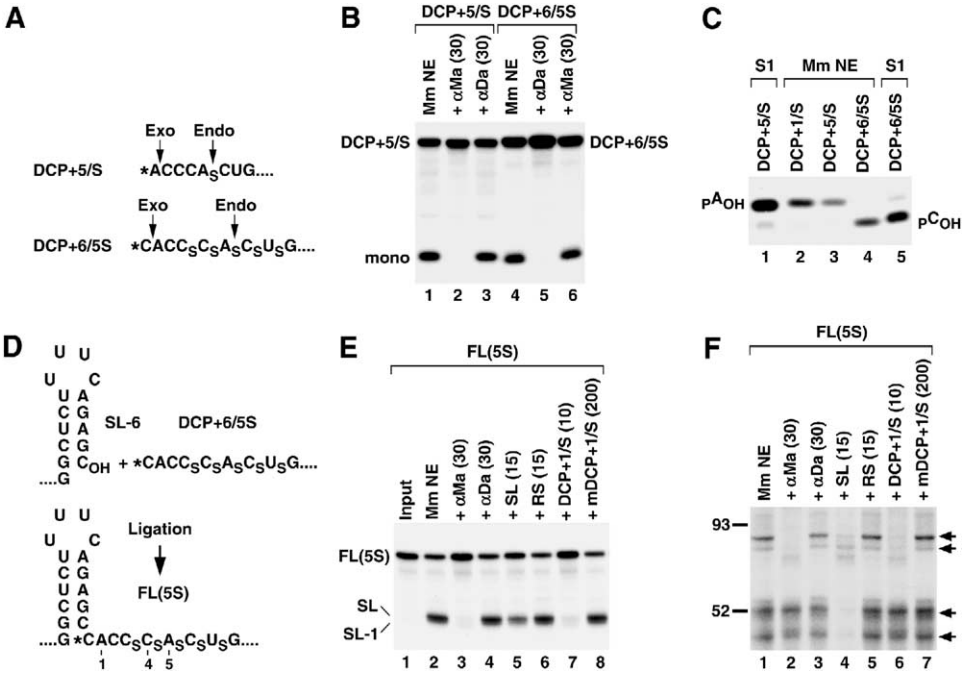

Figure 5. Distinguishing between the Endonucleolytic and the 5′-3′ Exonucleolytic Activities

(A) Partial sequences of the DCP+5/S and DCP+6/5S RNAs beginning with the most 5′ nucleotide. Phosphorothioate-modified bonds are indicated with S. Sites of the expected endonucleolytic cleavage (used in the full-length RNAs) and initial 5′ exonucleolytic attack are indicated with arrows. The labeled phosphate is represented by an asterisk.

(B) Release of the labeled mononucleotide from the 5′-labeled DCP+5/S (lanes 1–3) and DCP+6/5S RNAs (lane 4–6) in Mm NE. The numbers in parentheses indicate the amount of the RNA competitors in pmol.

(C) High-resolution gel electrophoresis of labeled mononucleotides released upon incubation of the indicated RNAs with S1 nuclease (lanes 1 and 5) or Mm NE (lanes 2–4).

(D) Diagram of construction of the FL(5S) RNA containing a radiolabeled phosphate (asterisk) within the stem and five phosphorothioate modifications (S) around the cleavage site. Only partial sequences of the SL-6 and DCP+6/5S RNAs used in ligation are shown. The nucleotides in the FL(5S) following the stem are numbered.

(E) In vitro processing of the FL(5S) RNA in Mm NE (lanes 2–8) in the presence of the indicated amounts (pmol) of competitors.

(F) Formation of UV crosslinks in the processing reactions shown in (E). Processing-dependent crosslinks are indicated with arrows.

ing the 5′ end further away from the HDE does not prevent the exonucleolytic activity dependent on the U7 snRNP and strongly suggests that the first nucleotide of DCP+1/S RNA is also removed by an exonucleolytic activity. The labeled mononucleotides released from the DCP+5/S and DCP+6/5S comigrated in a 14% high-resolution gel with the mononucleotides released after complete digestion of the two RNAs by S1 nuclease (Figure 5C), indicating that they contain a 3′ hydroxyl group (Sollner-Webb et al., 2001).

Cleaving of the FL(1S) RNA at the minor site 1 nucleotide upstream of the normal site containing the phosphorothioate generated 5′-labeled DCP+1/S, which was subsequently converted with about 50% efficiency into mononucleotides (Figure 2E). This raised a possibility that the 85 kDa crosslink was not formed during contact with the full-length RNA but instead was only formed after cleavage, during the degradation of the DCP+1/S, as observed in the case of the synthetic DCP+1/S RNA. Although this possibility seemed unlikely given the low efficiency of this pathway, we constructed a new full-length RNA by ligating the 5′-labeled DCP+6/5S with the SL lacking 6 nucleotides from the 3′ end (Figure 5D). In the FL(5S) RNA, the radioactive phosphate was placed within the stem, thus precluding any upstream cleavage that would have resulted in generation of a labeled downstream cleavage product. The purpose of the five phosphorothioate modifications was to allow detection of the crosslink in any possible cleavage site, which might be shifted 1 to 2 nucleotides in each direction.

The gel purified FL(5S) was efficiently cleaved in a mouse nuclear extract giving rise to two closely migrating upstream products (detectable with this substrate due to upstream position of the label), with the upper band being predominant (Figure 5E). In a high-resolution gel, the upper product comigrated with the major cleavage product of the site-specifically labeled FL(1S) RNA, and the minor product was 1 nucleotide shorter (data not shown). Thus, the FL(5S) RNA is cleaved at the same sites as the FL(1S). The processing was dependent on U7 snRNP and was competed by 100-fold molar excess of unlabeled DCP+1/S but not by the mutant version unable to bind U7 snRNP (Figure 5E, lanes 7 and 8). As expected, excess of the SL RNA reduced the efficiency of processing, and the RS had no effect (lanes 5 and 6). When the same processing reactions were UV irradiated and treated with RNase T1, the pat-

tern of crosslinked proteins looked very similar to that obtained with the FL(1S) RNA (Figure 5F). The main difference was that there was a doublet near 85 kDa rather than a single band (Figure 5F). The lower band comigrated with the 85 kDa crosslink formed on the DCP+1/S RNA (data not shown), whereas the more intense band had slightly lower mobility. Formation of this doublet crosslink correlated with processing efficiencies and responded to all competitors in the same manner as formation of the 85 kDa crosslink on the FL(1S) RNA (Figure 5F). Processing and formation of the doublet crosslink, but not stem-loop-dependent crosslinks, were also abolished by the presence of 0.05% NP-40 or 100-fold excess of the αHDEa blocking the U7 binding site (data not shown). This analysis suggested that the doublet may represent the same 85 kDa protein with the upper crosslink bound to a larger portion of the RNA due to incomplete digestion with RNase T1.

Immunoprecipitation of Crosslinked Proteins

Our studies demonstrated that the 85 kDa protein interacts with both the full-length histone pre-mRNA and the downstream cleavage product in a U7-dependent manner. The electrophoretic mobility of the 85 kDa protein indicated that this is a new factor in histone-pre-mRNA processing. To identify the 85 kDa protein, we initially used crosslinks formed on the DCP+1/S RNA due to its availability in large quantities and tested a number of antibodies against known proteins. We recently characterized a potential candidate for the endonuclease in 3′ end processing of histone pre-mRNAs as a heterodimer of RC-68 and RC-74 (Dominski et al., 2005), two proteins highly similar to CPSF-73 and CPSF-100. While RC-68 migrates at about 63 kDa, RC-74 has a mobility identical to the 85 kDa crosslink. We used an antibody against the C-terminal peptide of RC-74 and carried out immunoprecipitation under denaturing conditions. In this method, the sample containing the crosslinked proteins is treated with an RNase, boiled in the presence of 1% SDS, and then diluted 10-fold prior to addition of an antibody. This approach increases the efficiency of immunoprecipitation when the protein of interest is imbedded in a larger complex and therefore is not accessible to the antibody in a native form. The RC-74 antibody efficiently precipitated denatured RC-74, as determined by Western blotting, but did not precipitate any of the radioactive 85 kDa protein, demonstrating that the 85 kDa protein is not RC-74 (data not shown).

We next considered the possibility that the 85 kDa protein might be CPSF-73, the suspected cleavage factor in cleavage/polyadenylation, which also migrates on SDS gels near 85 kDa (Dominski et al., 2005). As determined by IP/Western, an αCPSF-73 antibody (kindly provided by Dr. W. Keller, University of Basel) was unable to precipitate CPSF-73 from a native nuclear extract (data not shown) but efficiently precipitated CPSF-73 from an extract denatured by boiling in the presence of SDS (Figure 6A, bottom panel, lanes 9 and 13). The αCPSF-73 antibody incubated with a UV-irradiated and denatured processing reaction containing the DCP+1/S RNA selectively precipitated the 85 kDa but not the 50 kDa protein, thus identifying the 85 kDa protein as CPSF-73 (Figure 6A, lane 3). Quantification of the data on a PhosphorImager demonstrated that over 25% of the input 85 kDa crosslink was precipitated with the αCPSF-73. The two control antibodies directed against RC-74 and RC-68 did not precipitate any labeled proteins (Figure 6A, lanes 2 and 4). We also analyzed a processing reaction prepared in the presence of the αMa oligonucleotide, which prevented formation of the 85 kDa UV crosslink but did not reduce the intensity of the 50 kDa band or the background (Figure 6A, lane 5). The αCPSF-73 antibody did not precipitate any radioactive protein from this sample (lane 6).

We repeated the above experiment using a different rabbit antibody against CPSF-73 (αCPSF-73b), kindly provided by Dr. D. Bentley (University of Colorado, Denver). We prepared a large-scale processing reaction with the DCP+1/S RNA either without (lanes 7–10) or

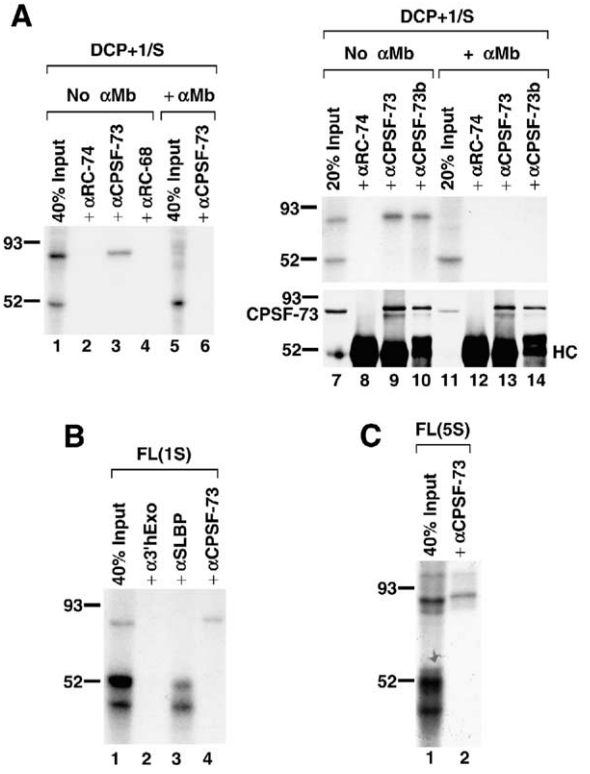

Figure 6. Immunoprecipitation of UV-Crosslinked Proteins

(A) Processing reactions containing the 5′-labeled DCP+1/S RNA were UV irradiated, treated with RNase A, denatured by boiling in the presence of SDS, and incubated with antibodies indicated at the top of each lane. The reactions were prepared either in the absence (No αMb) or presence of the αMb (+ αMb). The precipitated proteins were resolved in SDS gels and detected by autoradiography. The immunoprecipitation of CPSF-73 in samples shown in lanes 7–14 was monitored in parallel by Western blotting using αCPSF-73 (bottom panel). The position of the immunoglobulin heavy chain is indicated with HC.

(B and C) Processing reactions containing the site-specifically labeled FL(1S) (B) or FL(5S) RNAs (C) were prepared and processed as described in (A), with the exception that RNase T1 was used instead of RNase A. Note that the gel in (C) was run longer than other gels in (A) and (B), accounting for the larger distance between the 93 and 52 kDa size markers.

with the αMa oligonucleotide (lanes 11–14) and tested the αCPSF-73b antibody in parallel with the initial αCPSF-73. The results from these experiments were the same as described above: each of the two antibodies directed against CPSF-73 selectively precipitated the 85 kDa radioactive protein from the control processing reaction (Figure 6A, top, lanes 9 and 10), while the αRC-74 was unable to precipitate any radioactive protein (lane 8). The two αCPSF-73 antibodies did not precipitate any radioactive protein from processing reactions containing the αMa (lanes 13 and 14), although they efficiently precipitated CPSF-73 from aliquots of the same processing reactions, as determined by Western blotting (Figure 6A, lanes 13 and 14, bottom).

Finally, following the same denaturing protocol as that used for the DCP+1/S RNA, we determined that CPSF-73 was also crosslinked to the full-length substrates. To prevent removal of the label from crosslinked proteins, RNase T1 was used instead of RNase A. The αCPSF-73 antibody identified the 85 kDa protein crosslinked to the FL+1/S RNA as CPSF-73 (Figure 6B, lane 4), and the αSLBP antibody identified two crosslinks at 45 and 52 kDa as SLBP (Figure 6B, lane 3). While the 45 kDa crosslink migrates at position typical of SLBP, the slower form is most likely attached to a larger portion of the RNA protected against RNase T1 digestion by binding of SLBP. An antibody directed against the C-terminal peptide of 3′hExo, a 3′ exonuclease that specifically binds to the downstream side of the stem loop in the histone mRNA but not to the pre-mRNA (Dominski et al., 2003), did not precipitate any crosslinked protein (Figure 6B, lane 2). The αCPSF-73 antibody also precipitated the two crosslinks migrating at about 85 kDa formed in a processing-dependent manner on the FL(5S) RNA (Figure 6C, lanes 1 and 2). Thus, formation of the doublet was a result of the crosslinking of CPSF-73 to the RNA substrate followed by its incomplete digestion with RNase T1. In conclusion, we identified the 85 kDa protein crosslinked in a U7-dependent manner to the histone pre-mRNA and to the downstream cleavage product as CPSF-73, an essential component of the cleavage/polyadenylation apparatus.

Discussion

Histone-pre-mRNA processing requires binding of the U7 snRNP to the HDE located 12–15 nucleotides 3′ of the cleavage site. The U7 snRNP plays the key role in assembling the processing complex and functions as a molecular ruler directing the cleavage factor to the appropriate phosphodiester bond in the pre-mRNA (Scharl and Steitz, 1994). Two reactions are catalyzed by the processing complex containing the U7 snRNP: an endonucleolytic cleavage of histone pre-mRNA to form the 3′ end of histone mRNA and a 5′-to-3′ exonucleolytic degradation of the downstream cleavage product, which may play a role in recycling the U7 snRNP (Walther et al., 1998). In this study, we identified a protein of 85 kDa that crosslinks in a U7-dependent manner to the RNA substrates during both endonucleolytic cleavage and 5′-to-3′ exonucleolytic degradation. Immunoprecipitation experiments identified this protein as CPSF-73, a component of the cleavage/polyadenylation machinery recently proposed to function as the cleavage factor in formation of the polyadenylated mRNAs (Aravind, 1999; Callebaut et al., 2002; Ryan et al., 2004).

UV Crosslinking of CPSF-73 to the RNA Substrates Is Processing Dependent

We used two different 2′-O-methyl oligonucleotides complementary to the 5′ end of the mouse U7 snRNA, αMa and αMb, that specifically inhibit endonucleolytic cleavage of the full-length pre-mRNAs, FL(1S) and FL(5S), and 5′-3′ exonucleolytic degradation of the downstream cleavage product, DCP+1/S. Both oligonucleotides abolished UV crosslinking of CPSF-73 to these RNA substrates. The cleavage and degradation as well as crosslinking of CPSF-73 were also abolished by an excess of RNA containing the wild-type U7 binding site but not with RNAs unable to efficiently interact with the U7 snRNP. In addition to crosslinking of CPSF-73, we also detected crosslinking of SLBP to the full-length substrates and a 50 kDa protein to the DCP+1/S RNA. As expected, binding of SLBP to the full-length RNA was not inhibited by the addition of the αMa since SLBP interacts with the stem loop independently of U7 snRNP. We have previously demonstrated that SLBP stimulates binding of the U7 snRNP to the pre-mRNA and increases the efficiency of processing (Dominski et al., 1999). Consistent with these studies, sequestering SLBP reduced processing and crosslinking of CPSF-73. The competition experiments suggested that the 50 kDa protein is not essential for degradation of the DCP+1/S RNA. However, coprecipitation of the 50 kDa crosslink by the anti-Sm antibody suggests that it may be a part of a larger complex with the U7 snRNP or another Sm-precipitable particle (Figure S2). Additional studies are required to determine the identity and the relevance, if any, of this protein to 3′ end processing of histone pre-mRNAs.

The key modification that allowed UV crosslinking of CPSF-73 was incorporation of a phosphorothioate at the cleavage site in the full-length RNA or near the 5′ end of the DCP. RNA substrates lacking this modification, in spite of undergoing very rapid processing, did not crosslink to any protein in a processing-specific manner. Introduction of a single phosphorothioate did not significantly reduce the overall efficiency of processing or degradation, which is probably limited by the rate of assembly of the U7 snRNP and other necessary factors on the RNA substrate. However, this modification likely slowed down the rate of the nucleolytic attack, allowing CPSF-73 to stay longer in contact with the RNA. The presence of the phosphorothioate in the cleavage site in the full-length RNA did not prevent processing in this site, although it resulted in generation of a minor cleavage site 1 nucleotide upstream, indicating that this modification creates an at least partially unfavorable context for processing.

CPSF-73 Is a Primary Candidate for 3′ Endonuclease in Formation of Histone RNAs and Polyadenylated mRNAs

Crosslinking of CPSF-73 only in the presence of the phosphorothioate modification in RNA substrates, in-

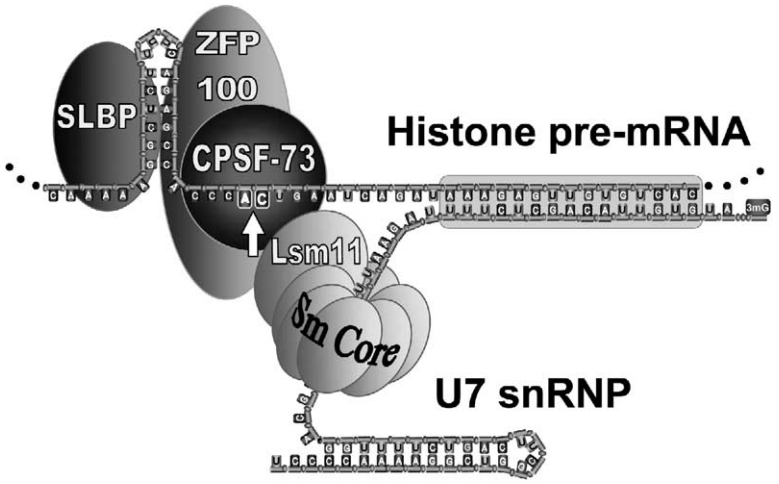

Figure 7. 3′ End Processing of Histone Pre-mRNAs

Components of the 3′ end-processing machinery cleaving histone pre-mRNAs and known or predicted interactions within the complex. Lsm10 in the unique U7 Sm core complex is not indicated. The complex may contain other proteins, possibly CPSF-100 (not shown).

dicative of the transient nature of the interaction, strongly suggests CPSF-73 is the cleavage factor in 3′ end processing of histone pre-mRNAs. However, the ultimate proof of this function will require purification of CPSF-73, and possibly auxiliary proteins, and direct demonstration that it displays nucleolytic activity in vitro.

The role of CPSF-73 as the endonuclease in 3′ end processing in histone pre-mRNAs is supported by structural features of this protein characterized by the presence of the β-CASP domain typical of a small group of proteins with either predicted or proven nuclease activity (Callebaut et al., 2002). This group includes two DNA-specific nucleases: Artemis, involved in V(D)J recombination and DNA double-strand break repair (Moshous et al., 2001), and SNM1, involved in DNA crosslink repair (Dronkert et al., 2000). Within a small region flanking the catalytic histidine motif, CPSF-73 is also similar to ELAC1 and ELAC2, two related endonucleases required for 3′ end processing of pre-tRNAs (Takaku et al., 2003). Notably, two β-CASP domain proteins distantly related to CPSF-73 have recently been identified in *Bacillus.* These proteins, RNase J1 and J2, are involved in maturation of specific mRNAs in vivo and display in vitro endonucleolytic activity on RNA substrates (Even et al., 2005).

A growing amount of circumstantial evidence suggests that CPSF-73 is the endonuclease in formation of polyadenylated mRNAs. However, crosslinking experiments with a site-specifically labeled pre-mRNA substrate failed to detect this protein at the cleavage site (Ryan et al., 2004). Despite using different sequence elements and factors that recognize these elements, 3′ end processing of histone pre-mRNAs and cleavage coupled to polyadenylation exhibit some striking similarities. Both types of pre-mRNA contain two sequence elements required for processing, and cleavage occurs between the two sequence elements, preferentially after an adenosine. The precise position of the cleavage site in both types of pre-mRNA is not absolute and can be shifted to a less preferable nucleotide by changing the spacing between the two elements (Chen et al., 1995; Scharl and Steitz, 1994). Following the endonucleolytic cleavage, the upstream fragment corresponds to the mature mRNA, whereas the downstream fragment is converted into a group of truncated products differing in location of the 5′ end (Sheets et al., 1987; Walther et al., 1998). Finally, both processing reactions are resistant to EDTA and generate a hydroxyl group at the 3′ end typical of metal-mediated catalysis (Gick et al., 1986; Moore and Sharp, 1985; Wahle and Keller, 1996).

CPSF-73 Is Likely Both the Endonuclease and 5′-3′ Exonuclease in 3′ End Processing

CPSF-73 crosslinked in a U7-dependent manner to both full-length RNAs and to the downstream cleavage product. These results strongly suggest that CPSF-73 is both the endonuclease generating the correct 3′ end of histone mRNAs and the 5′ exonuclease responsible for release of the U7 snRNP. It is possible that the 5′-to-3′ mode requires the proximity of the 5′ phosphate. It will be interesting to determine how long of an extension at the 5′ end would still allow the 5′-3′ activity to degrade the RNA. We predict that moving the 5′ end sufficiently far away from the U7 binding site could prevent the exonucleolytic activity and result in switching to the endonucleolytic mode. Our interpretation that CPSF-73 carries both activities is supported by their similar reaction requirements. The cleavage of the FL pre-mRNA and the degradation of the DCP occur in the presence of high concentrations of EDTA when most nuclear nucleases are inactive. In addition, both activities display similar sensitivity to low concentrations of NP-40 and increased concentrations of KCl (data not shown). Interestingly, Artemis, a β-lactamase fold protein sharing the β-CASP domain with CPSF-73, in vitro is a 5′-3′ exonuclease and in complex with the DNA-dependent protein kinase acts as endonuclease (Ma et al., 2002). CPSF-73 may also require a second protein, for example CPSF-100, to display its endonucleolytic activity.

Mechanistic and Evolutionary Considerations

Identification of CPSF-73 as the likely endonuclease in formation of mature histone mRNAs raises a number of important questions. How is CPSF-73 recruited to the

cleavage site by the two vastly different processing machineries, which do not share any other known factor and assemble on the two vastly different pre-mRNA substrates? In cleavage/polyadenylation, CPSF-73 is recruited to the vicinity of the cleavage site by CPSF-160 that recognizes the AAUAAA. It is therefore unlikely that CPSF-160 is involved in histone-pre-mRNA processing. Indeed, crosslinking of CPSF-73 to the DCP+1/S or FL(5S) was not competed by excess of an RNA containing the AAUAAA (Figure S3). CPSF-73 is most likely recruited to the histone pre-mRNA by binding to a specific U7 snRNP protein, with two primary candidates being either Lsm 11 or ZFP100 (Figure 7). CPSF-73 directly interacts with a related protein, CPSF-100, in which the catalytic histidine motif is disrupted (Dominski et al., 2005). It is possible that CPSF-100 is a mediator in recruiting CPSF-73 to the U7 snRNA and the cleavage site.

The involvement of CPSF-73 in formation of the mature histone mRNAs and polyadenylated mRNAs may suggest that the two 3′ end processing mechanisms are distantly related and evolved from common primordial machinery. The most striking difference between the two mechanisms is the requirement for an RNA-containing factor in histone-pre-mRNA processing and the lack of an RNA component in cleavage/polyadenylation. Thus, 3′ end processing of histone pre-mRNAs may represent a more primitive reaction than cleavage and polyadenylation, which may have evolved into an entirely protein-based mechanism (Mowry and Steitz, 1988).

Experimental Procedures

RNAs

All RNA substrates used in crosslinking experiments and 2′-O-methyl oligonucleotide competitors were synthesized by Dharmacon, and their sequences are shown in Figure 2. Full-length pre-mRNA substrates were generated by T7 RNA transcription, gel purified, and quantified.

RNA Labeling

Most RNA substrates were labeled at the 5′ end using T4 polynucleotide kinase (NEB) and 30 μCi of [γ-^{32}P]ATP. Internally labeled RNA substrates were synthesized by incorporation of [^{32}P]αUTP in the presence of T7 RNA polymerase, as described (Dominski et al., 1999).

RNA Ligation

The site-specifically labeled full-length pre-mRNA substrate was generated by joining two RNA segments, essentially as described (Moore and Query, 2000).

Preparation of Nuclear Extracts

Nuclear extracts from mouse myeloma and HeLa cells grown at the National Cell Culture Center (Minneapolis) were prepared as previously described (Dominski et al., 1999).

UV Crosslinking

Each reaction used in crosslinking experiments was set up on ice in a final volume of 20 μl and contained the following: 0.1 pmol of labeled RNA, 20 mM EDTA, 5 μg of yeast tRNA, and 15 μl of a nuclear extract (~10 μg protein/μl). Unless otherwise indicated, the samples were preincubated for 10 min at 32°C, and 15 μl were placed on parafilm and irradiated for 8 min at room temperature with 1 J of UV (254 nm) from a distance of 2 in using UV Stratalinker 2400 (Stratagene). The remaining 5 μl portion of each reaction was incubated for an additional 80 min at 32°C and analyzed for processing efficiency by separating the reaction products in an 8% polyacrylamide/7 M urea gel. Unless otherwise indicated, the UV-irradiated samples containing the full-length RNA (FL), DCP+1/S, or DCP+1 were treated with 20 μg of RNase A. The samples containing the FL(1S) and the FL(5S) were treated with 2000 units of RNase T1 (Ambion). The samples treated with the appropriate RNase were resolved in a 12% SDS-polyacrylamide gel and analyzed by autoradiography.

Detection of U7 snRNA

Formation and immunoprecipitation of processing complexes by anti-SLBP in the absence or in the presence of 0.1% NP-40 and detection of the mouse U7 snRNA by Northern blotting were carried out as previously described (Dominski et al., 1999).

Immunoprecipitation

To immunoprecipitate denatured proteins, 25 μl processing reactions irradiated with UV were treated for 4 hr with either RNase A or T1, mixed with the same volume of 2× SDS buffer (2% SDS, 20 mM Tris-HCl [pH 7.5]), and boiled for 5 min. The samples were supplemented with 200 μl of water and 250 μl of 2× IP buffer (20 mM Tris [pH 7.5], 300 mM NaCl, 2 mM EDTA, 1% NP-40, 2% Triton X-100) and used for immunoprecipitation with 2.5–5.0 μl of appropriate antibody. The samples were rotated at 4°C for 18 hr and subsequently transferred to new tubes containing 25 μl of protein A agarose beads. After 2.5 hr of rotation at 4°C, the beads were collected by gentle centrifugation and washed several times with 1× IP buffer for a total of 1 hr. Proteins absorbed on the beads were recovered by boiling with SDS loading dye and separated on 12% SDS-polyacrylamide gels.

Supplemental Data

Supplemental Data include three figures and can be found with this article online at http://www.cell.com/cgi/content/full/123/1/37/DC1/.

Acknowledgments

This work was supported by NIH grant GM29832 to W.F.M. We thank M. Purdy for excellent technical assistance and S. Whitfield (UNC Chapel Hill) and P. Spychala (ScienceSlides by Visiscience Inc.) for help with the figures. We are grateful to Dr. W. Keller (University of Basel) and Dr. D. Bentley, (University of Colorado, Denver) for antibodies against CPSF-73.

Received: May 6, 2005
Revised: July 8, 2005
Accepted: August 3, 2005
Published Online: September 29, 2005

References

Aravind, L. (1999). An evolutionary classification of the metallo-beta-lactamase fold proteins. In Silico Biol. *1*, 69–91.

Birnstiel, M.L., and Schaufele, F.J. (1988). Structure and function of minor snRNPs. In Structure and Function of Major and Minor Small Ribonucleoprotein Particles, M.L. Birnstiel, ed. (Berlin: Springer-Verlag), pp. 155–182.

Bond, U.M., Yario, T.A., and Steitz, J.A. (1991). Multiple processing-defective mutations in a mammalian histone premessenger RNA are suppressed by compensatory changes in U7 RNA both in vivo and in vitro. Genes Dev. *5*, 1709–1722.

Callebaut, I., Moshous, D., Mornon, J.P., and De Villartay, J.P. (2002). Metallo-beta-lactamase fold within nucleic acids processing enzymes: the beta-CASP family. Nucleic Acids Res. *30*, 3592–3601.

Chen, F., MacDonald, C.C., and Wilusz, J. (1995). Cleavage site determinants in the mammalian polyadenylation signal. Nucleic Acids Res. *23*, 2614–2620.

Colgan, D.F., and Manley, J.L. (1997). Mechanism and regulation of mRNA polyadenylation. Genes Dev. *11*, 2755–2766.

Dominski, Z., and Marzluff, W.F. (1999). Formation of the 3′ end of histone mRNA. Gene *239*, 1–14.

Dominski, Z., Zheng, L.-X., Sanchez, R., and Marzluff, W.F. (1999). The stem-loop binding protein facilitates 3′ end formation by stabilizing U7 snRNP binding to the histone pre-mRNA. Mol. Cell. Biol. *19*, 3561–3570.

Dominski, Z., Erkmann, J.A., Yang, X., Sanchez, R., and Marzluff, W.F. (2002). A novel zinc finger protein is associated with U7 snRNP and interacts with the stem-loop binding protein in the histone pre-mRNP to stimulate 3′-end processing. Genes Dev. *16*, 58–71.

Dominski, Z., Yang, X., Kaygun, H., and Marzluff, W.F. (2003). A 3′ exonuclease that specifically interacts with the 3′ end of histone mRNA. Mol. Cell *12*, 295–305.

Dominski, Z., Yang, X.C., Purdy, M., Wagner, E.J., and Marzluff, W.F. (2005). A CPSF-73 homologue is required for cell cycle progression but not cell growth and interacts with a protein having features of CPSF-100. Mol. Cell. Biol. *25*, 1489–1500.

Dronkert, M.L., de Wit, J., Boeve, M., Vasconcelos, M.L., Van Steeg, H., Tan, T.L., Hoeijmakers, J.H., and Kanaar, R. (2000). Disruption of mouse SNM1 causes increased sensitivity to the DNA interstrand cross-linking agent mitomycin C. Mol. Cell. Biol. *20*, 4553–4561.

Even, S., Pellegrini, O., Zig, L., Labas, V., Vinh, J., Brechemmier-Baey, D., and Putzer, H. (2005). Ribonucleases J1 and J2: two novel endoribonucleases in B.subtilis with functional homology to E.coli RNase E. Nucleic Acids Res. *33*, 2141–2152.

Gick, O., Krämer, A., Keller, W., and Birnstiel, M.L. (1986). Generation of histone mRNA 3′ ends by endonucleolytic cleavage of the pre-mRNA in a snRNP-dependent in vitro reaction. EMBO J. *5*, 1319–1326.

Koziolkiewicz, M., Wojcik, M., Kobylanska, A., Karwowski, B., Rebowska, B., Guga, P., and Stec, W.J. (1997). Stability of stereoregular oligo(nucleoside phosphorothioate)s in human plasma: diastereoselectivity of plasma 3′-exonuclease. Antisense Nucleic Acid Drug Dev. *7*, 43–48.

Ma, Y., Pannicke, U., Schwarz, K., and Lieber, M.R. (2002). Hairpin opening and overhang processing by an Artemis/DNA-dependent protein kinase complex in nonhomologous end joining and V(D)J recombination. Cell *108*, 781–794.

Moore, C.L., and Sharp, P.A. (1985). Accurate cleavage and polyadenylation of exogenous RNA substrate. Cell *41*, 845–855.

Moore, M.J., and Query, C.C. (2000). Joining of RNAs by splinted ligation. Methods Enzymol. *317*, 109–123.

Moshous, D., Callebaut, I., De Chasseval, R., Corneo, B., Cavazzana-Calvo, M., Le Deist, F., Tezcan, I., Sanal, O., Bertrand, Y., Philippe, N., et al. (2001). Artemis, a novel DNA double-strand break repair/V(D)J recombination protein, is mutated in human severe combined immune deficiency. Cell *105*, 177–186.

Mowry, K.L., and Steitz, J.A. (1988). snRNP mediators of 3′ end processing: functional fossils? Trends Biochem. Sci. *13*, 447–451.

Ryan, K., Calvo, O., and Manley, J.L. (2004). Evidence that polyadenylation factor CPSF-73 is the mRNA 3′ processing endonuclease. RNA *10*, 565–573.

Scharl, E.C., and Steitz, J.A. (1994). The site of 3′ end formation of histone messenger RNA is a fixed distance from the downstream element recognized by the U7 snRNP. EMBO J. *13*, 2432–2440.

Schumperli, D., and Pillai, R.S. (2004). The special Sm core structure of the U7 snRNP: far-reaching significance of a small nuclear ribonucleoprotein. Cell. Mol. Life Sci. *61*, 2560–2570.

Sheets, M.D., Stephenson, P., and Wickens, M.P. (1987). Products of in vitro cleavage and polyadenylation of simian virus 40 late pre-mRNAs. Mol. Cell. Biol. *7*, 1518–1529.

Sollner-Webb, B., Cruz-Reyes, J., and Rusche, L.N. (2001). Direct sizing of RNA fragments using RNase-generated standards. Methods Enzymol. *342*, 378–383.

Takaku, H., Minagawa, A., Takagi, M., and Nashimoto, M. (2003). A candidate prostate cancer susceptibility gene encodes tRNA 3′ processing endoribonuclease. Nucleic Acids Res. *31*, 2272–2278.

Wahle, E., and Keller, W. (1996). The biochemistry of polyadenylation. Trends Biochem. Sci. *21*, 247–250.

Walther, T.N., Wittop, K.T., Schümperli, D., and Muller, B. (1998). A 5′-3′ exonuclease activity involved in forming the 3′ products of histone pre-mRNA processing in vitro. RNA *4*, 1034–1046.

Zhao, J., Hyman, L., and Moore, C. (1999). Formation of mRNA 3′ ends in eukaryotes: mechanism, regulation, and interrelationships with other steps in mRNA synthesis. Microbiol. Mol. Biol. Rev. *63*, 405–445.